OPTOELECTRONICS AND ADVANCED MATERIALS – RAPID COMMUNICATIONS Vol. 3, No. 12, December 2009, p. 1285 - 1289

Size dependent structural, optical and magnetic properties of un-doped SnO_2 nanoparticles

A. SHARMA*, S. KUMAR[a], R. KUMAR[b], M. VARSHNEY, K. D. VERMA
Material Science Research Laboratory, Department of Physics, S.V.College, Aligarh-202001 (U.P) India
[a]*School of Nano and Advanced Materials Engineering Changwon National University #9 Sarim-Dong, Changwon, 641-773, Republic of Korea*
[b]*Inter University Accelerator Center, Aruna Asaf Ali Marg, New Delhi-110067, India*

Nanosized tin oxide (SnO_2) powders of different sizes were synthesized using co-precipitation method without using any surfactant or capping agent. The crystal structure, morphology, optical band gap and magnetic behavior of so formed SnO_2 nanoparticles were investigated by using, x-ray diffraction (XRD), transmission electron microscopy (TEM), UV-visible absorption, and magnetic hysteresis loop measurements. Room temperature ferromagnetism with a significant blue shift in absorption edge was observed in 3pH grown sample. The controlled colloidal synthesis, with pH variation, and post annealing process grown larger sized nanoparticles have shown size dependent magnetic characteristics and sufficient red-shift in the absorption edge. The grain growth processes during colloidal synthesis and post annealing are also briefed.
Keywords: SnO_2, nanoparticles, ferromagnetism, diamagnetism, x-ray diffraction.

(Received November 01, 2009; accepted November 23, 2009)

Keywords: Nanoparticles, XRD, TEM, ferromagnetism and grain growth

1. Introduction

Crystal growth has been studied extensively and this topic has recently gained even greater importance due to interest in controlling particle size of nanostructured materials [1-5]. Several methods of synthesizing metal, semiconductor and metal oxide nanostructures have been demonstrated, including template-based growth [6], thermal evaporation [7] and plasma-molecular beam epitaxy [8] etc. Most of these methods do not yield a single phase material with significant amount of nanoparticles with narrow size distribution. The difficulties involved in obtaining a high quality and controlled size/shape nanoparticles have prevented the investigations on their diversifying properties. More recently, room temperature ferromagnetism has been reported in un-doped SnO_2 nanoparticles and thin films [9-10], but not in bulk. This kind of observation challenges the conventional understanding of ferromagnetism, which is rather due to spin-split states or bands. In spite of the progress in the developing oxide based ferromagnetic semiconductors, there has been a much controversy concerning the mechanism that causes the magnetism in these systems [11-12]. Intensive theoretical work has been performed to understand the ferromagnetism in nanostructured and defective oxides [10-13]. In these reports, the triplet states of p-like electrons, located at cation or oxygen vacancies, yield the local moments, leading to a kind of ferromagnetism without the involvement of 3d electrons.

In order to understand the size dependent physical properties of un-doped SnO_2 nanoparticles, we have employed a pH controlled wet chemical method by which SnO_2 nanoparticles, having different sizes, are synthesized at low temperature without requiring any surfactant or capping agent. Post annealing treatment was also employed on as prepared powders to further increase the size of SnO_2 nanoparticles. Our choice of SnO_2 as the test material was based on its very low solubility in the solvent used during synthesis, particularly at low temperatures. Besides this, SnO_2 is a wide band gap semiconductor that presents interesting optical, magnetic and electrical properties [14-15].

2. Experimental details

All the reagents used were of analytical grade without further purification. Ammonium Hydroxide was added (drop wise) into the $SnCl_4.5H_2O$ molar solution (0.01M) with stirring. The pH value was controlled via controlling the NH_4OH concentration in the solution. The resultant white precipitates were rinsed with de-ionized water and dried in air at 40 ^{0}C. Some part of the powder product, grown at 7pH, was annealed in air at 800 ^{0}C for four hours. Powder x-ray diffraction was carried out with Bruker D8 advanced diffractometer using Cu-Ka radiation (λ = 1.540Å). The microstructures were studied with FEI-Tecnai-20 transmission electron microscope, operated at 200 kV. Optical absorption spectra were recorded with the conventional two beam method using Varian Carry-5000, UV-VIS-NIR spectrometer in the wavelength range of 225– 600nm. Magnetic hysteresis loop measurements were performed at room temperature using a super conducting quantum interference device (SQUID) magnetometer (Quantum Design, PPMS).

3. Results and discussion

Fig. 1 shows the x-ray diffraction pattern of; (a) 3pH grown, (b) 7pH and (c) 800 ^{0}C annealed tin oxide nanoparticles, respectively. It is clearly evident from the Fig.1 that all the observed peaks are corresponding to rutile-type SnO_2 (space group, $P4_2/mnm$, PDF- 72 # 721147) with a preferred orientation in (110) plane. This is because the (110) surface present minimum surface energy compared to other surfaces [16]. The full width at half maxima (FWHM) and intensity, estimated from (110) peak of all the samples, shows systematic variation with increasing the pH value and annealing of the samples. The estimated FWHM (in radian) are 4.21, 2.02 and 0.229 for 3pH grown, 7pH grown and annealed SnO_2 nanoparticles, respectively. The decrease in FWHM and increase in the peak intensities could be due to the improvement in the crystallinity of the pockets of amorphous zones and the grain growth of the original crystalline phase. The average grain size estimated from the XRD peaks using Scherrer relation ($D = 0.9\ \lambda/\beta\ \cos\theta$) are 1.89 nm, 3.94 nm and 35.2 nm for 3 pH grown, 7 pH grown and annealed nanoparticles, respectively. The lattice parameters were calculated using the equation:

$$\frac{1}{d^2} = \frac{h^2 + k^2}{a^2} + \frac{l^2}{c^2}, \qquad (1)$$

where, a and c are the unit cell parameters, d is the inter-planner distance. Thus calculated lattice parameter are; a = 4.740Å, 4.738Å and 4.736Å for 3pH, 7pH and annealed samples, respectively. It is clear from the above calculations that particle size has strong relation with WFHM of the XRD peaks and the lattice parameters of SnO_2 nanocrystals. Furthermore, the lattice parameters of 3 pH grown SnO_2 nanoparticles were higher than that of bulk SnO_2 lattice parameters. For example, the lattice parameter for 3pH grown SnO_2 nanoparticles, calculated form XRD data, is a = 4.740Å whereas that of the corresponding bulk is 4.737 Å (PDF- 72 # 721147). This is an agreement with earlier reports that the lattice expands in oxide nanoparticles due to the presence of oxygen ion vacancies or due to the variation in ionicity of the metal oxide semiconductors [17]. These results reveal that the particle size has a great impact on the structural properties of tin oxide nanoparticles.

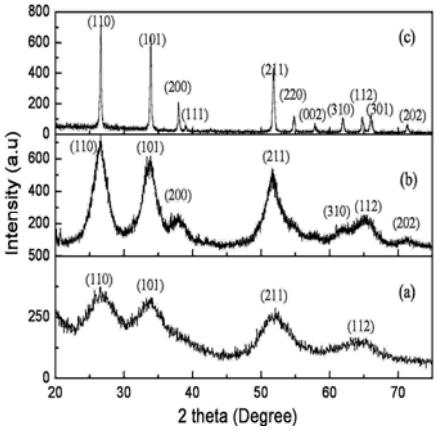

Fig. 1. X-ray diffraction patterns of (a) 3pH grown (b) 7pH grown and (c) annealed SnO_2 nanoparticles.

Fig. 2 (a), (b) and (c) show the TEM micrograph of 3 pH grown, 7 pH grown and annealed tin oxide nanoparticles, respectively. Fig. 2(a) and (b) depict the presence of spherical shaped nanoparticles in 3pH and 7pH grown samples suggesting the wet chemical method, employed in this work, has controlled the morphology of nanoparticles without using any surfactant or capping agent. Fig. 2 (c) shows that the SnO_2 nanoparticles are converted into agglomerated lumps and larger sized nanoparticles due to annealing process. The size estimated from individual spherical shaped nanoparticles is about to 1.75 nm, 4.02 nm and 33.7 nm for 3 pH grown, 7 pH grown and annealed tin oxide nanoparticles, respectively. These results are in good agreement with those obtained from XRD analysis.

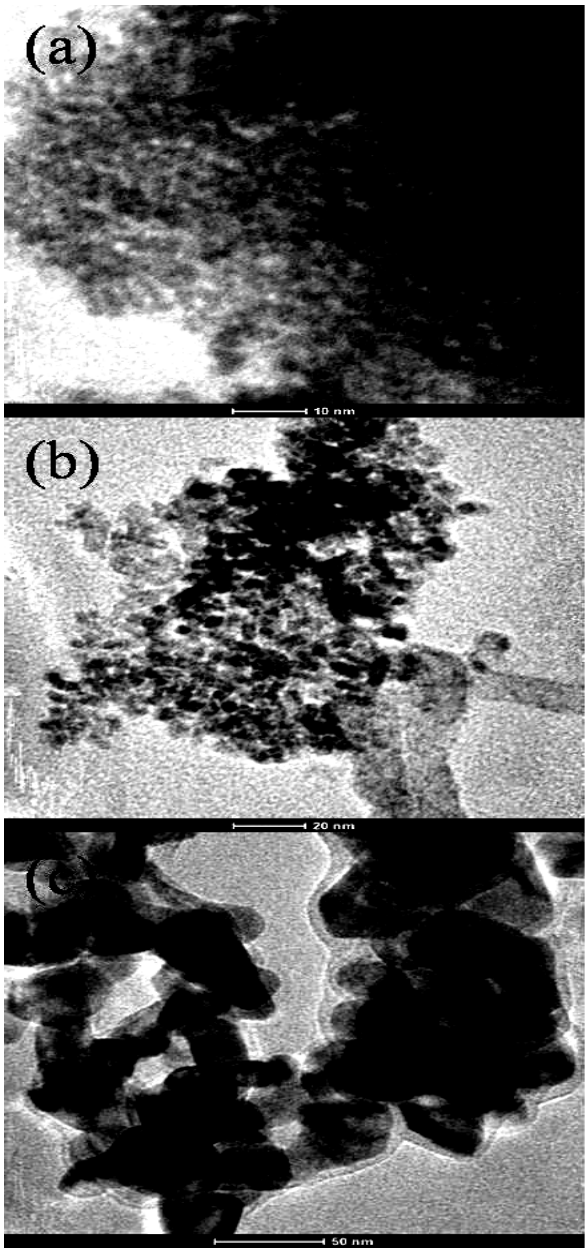

Fig. 2. TEM micrographs of (a) 3pH grown (b) 7pH grown and (c) annealed SnO_2 nanoparticles.

UV-visible spectroscopy is an important tool for optical characterization of materials. It provides useful information about the optical band gap of the semiconductors. For the semiconductor nanoparticles, the quantum confinement effect is expected and the absorption edge will be shifted to a higher energy when the particle size decreases [4, 18]. To correlate microstructures with the optical properties of the 3pH grown, 7pH grown and annealed nanoparticles, systematic UV-visible optical absorption studies were carried out on the samples. Fig. 3 shows the Tauc's plot by plotting $(\alpha h\nu)^2$ versus $(h\nu)$ and extrapolating the linear portion of the absorption edge to find the intercept with energy axis of (a) 3pH grown, (b) 7pH grown and (c) annealed SnO_2 nanoparticles. Inset of the figure shows absorption spectra of the same samples. A sufficient broadening of the absorption edge has been observed in case of annealed SnO_2 nanoparticles, which may arise due to inhomogeneous size distribution of nanoparticles. As reported earlier by Soumen Das, *et al*. [18]. The band gap of the 3pH grown, 7pH grown and annealed nanoparticles has been calculated from the Tauc's plots. The estimated band gap energies are 4.79 eV, 4.73 eV, and 3.66 eV for 3pH grown, 7pH grown and annealed SnO_2 nanoparticles, respectively. It is clear from the figure that significant red-shift in the absorption edge and thus smaller band gap have been observed in case of 7pH grown and annealed SnO_2 nanoparticles. The decrease in the band gap energy in the 7pH grown and annealed SnO_2 nanoparticles may arise due to the formation of larger sized nanoparticles and aggregated lumps during the colloidal synthesis and annealing process, respectively. The 3pH and 7pH grown samples exhibit 1.19 eV and 1.03 eV blue shift in the absorption spectra, comparison to the bulk band gap (3.6 eV) of SnO_2. This observed blue shift in case of 3pH and 4pH grown SnO_2 nanoparticles can be ascribed to the effect of the particle size (i.e., quantum confinement phenomenon), since the mean particle size of 3pH grown sample is closed to the value of the exciton Bohar radius of tin oxide (~2.7 nm) [4]. The band gap energy of annealed nanoparticles is very close to that of the bulk band gap energy of tin oxide because of their larger size (~ 35 nm). The TEM images corroborate these facts very well, as discussed earlier. Therefore, the engineering of nanoparticles size may provide a possibility of tunable semiconducting properties of tin oxide.

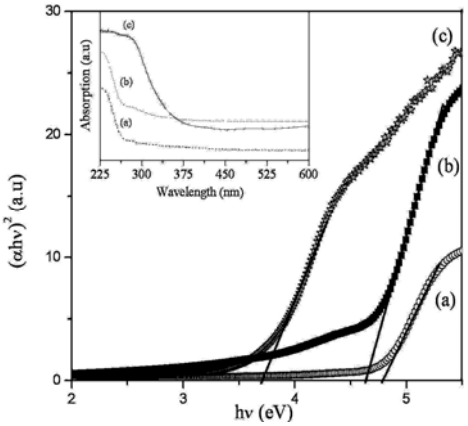

Fig. 3. Tauc's plot of (a) 3pH grown (b) 7pH grown and (c) annealed SnO_2 nanoparticles. Inset shows the UV-visible absorption of the same samples.

In order to investigate magnetic properties of (a) 3pH grown (b) 7pH grown and (c) annealed SnO_2 nanopaticles, systematic magnetization hysteresis loop were recorded at room temperature as shown in Fig. 4. It is clear from the figure that the 3pH grown sample shows significant ferromagnetic behavior with saturation magnetization of 4.7×10^{-4} emu/g, but other two samples of 7pH grown and annealed nanoparticles exhibit diamagnetic contribution at high field values. One should notice that the observed ferromagnetism in pure SnO_2 nanoparticles is very similar to the case of TiO_2, HfO_2, In_2O_3 and ZnO thin films and nanostructures [9-10, 19-21]. This amazing feature of ferromagnetism in pristine SnO_2 could be observed uniquely in thin films/nanostructures but not in bulk [22]. Since, there is no reason to attribute the introduction of ferromagnetism to any dopant, and moreover, in this SnO_2 case, there is no 3d electron involved, one cannot think of any interaction that may originate from that. Thus, we must reconsider the possibility that was previously assumed for the other ferromagnetic un-doped oxides: ferromagnetism due to oxygen vacancies and/or defects and confinement effects [22-23]. As for SnO_2, it seems that both factors are equally important. Few groups reported that their films of SnO_2 are diamagnetic [22], while ours 3pH grown SnO_2 nanoparticles are entirely ferromagnetic. Hays et al. reported that nanoparticles of SnO_2 are non-ferromagnetic [24], while Sundarsen et al have confirmed their SnO_2 nanoparticles are weakly ferromagnetic with some paramagnetic component. It is clear from the Fig. 4 that ferromagnetic contribution has decreased and diamagnetic contribution increases with increasing the size of SnO_2 nanoparticles. The diamagnetic behavior, observed at higher field values, may arises due to the diamagnetic contributions from the core of the SnO_2 nanoparticles, as core material of tin oxide is diamagnetic in nature, because, 4+ valance state of tin (Sn^{4+}) favors $4d^{10}$ electronic configuration of Sn in SnO_2. Similar diamagnetic contributions were also observed from the core of sintered ZnO nanoparticles [15]. Therefore, the origin of ferromagnetism in 3pH grown SnO_2 nanoparticles and diamagnetic contributions in 7pH grown and annealed SnO_2 nanoparticles are strongly related to their size and seems to be very similar to that of reported results by Sundarsen *et. al*. [25]. Here we also believe that the un-paired electron spins are responsible for ferromagnetism in the SnO_2 nanoparticles have their origin in the oxygen vacancies. In our XRD studies higher lattice parameter values for 3pH grown sample has been observed which may arises due to the presence of oxygen vacancies in the system [17]. It has been shown that, in the extreme case of single crystal SnO_2, surface reconstruction in the (110) surface involves up to three mono-layers of atoms and the presence of oxygen vacancies [26]. These results strengthen the fact of F-center mediated ferromagnetism in 3pH grown SnO_2 nanoparticles. An F center consists of an electron trapped in oxygen vacancy. The electron trapped in oxygen vacancy can occupy an orbital which overlaps electronic shells of two neighboring metal atoms and according to Hunds rule and Pauli Exclusion Principle, spin orientations of trapped electron and two neighboring metal ions become parallel in same direction leading to ferromagnetic ordering, present in 3pH grown sample. For F centers, the radius of the electron orbital is given by $\sim a_0\varepsilon$, where a_0 is the Bohr radius and ε is dielectric constant of the material. In SnO_2, $\varepsilon = 14$ [19], the radius of the F electron orbital is estimated to ~7.4 Å, which is

sufficiently large to mediate ferromagnetic coupling in the system. The magnetic properties of our SnO_2 samples may be related to their growth processes and synthesis conditions, therefore we tried to understand the growth processes of as-grown and annealed nanoparticles. From the nature of synthesis and experimental findings, the formation of SnO_2 nanoparticles in colloidal medium may occur as follows:

$$n(SnCl_4) + m(NH_4OH) \rightarrow nSn^{+4} + mNH_4^+ + mOH^- + 4nCl^- \quad (1)$$

$$nSn^{+4} + m(OH)^- \rightarrow xSn(OH)_2 \quad (2)$$

$$xSn(OH)_2 \xrightarrow{40^0 C(air)} ySnO_2 \downarrow + zH_2O \uparrow \quad (3)$$

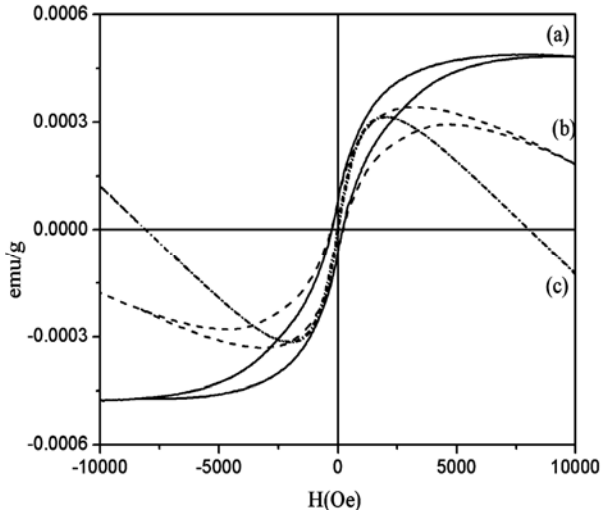

Fig. 4. Room temperature hysteresis curves of (a) 3pH grown (b) 7pH grown and (c) annealed SnO_2 nanoparticles.

In the step (i) of reaction, tin chloride and ammonium hydroxide underwent dissociation by ionic reaction, and form Sn^{+4}, OH^-, Cl^- and NH^{4+} ions. The step (iii) of reaction represents the formation of SnO_2 granules in the colloidal medium from the intermediate complex $Sn(OH)_2$ without addition of any surfactant or complexing agent. During the hydrothermal stage, so formed tin oxide granules are expected to collide and accordingly lay the foundations for the growth of SnO_2 nanoparticles. According to the GRIGC mechanism [3], when two or more granules collide, attachment between them is expected due to jiggling of granules by the Brownian motion. This process of attachment followed by the rotation of granules leading to the coalescence of neighboring grains via elimination of common grain boundaries [3], will acquire a lowest surface energy configuration and thereby formation of spherical shaped tin oxide nanoparticles being observed in 3pH grown sample. As the concentration of NH_4OH, and thus pH value, increases in the colloidal medium, the tin cations and hydroxide anions are expected to attach pronouncedly. Therefore, formation of higher concentration of intermediate complex, $(Sn(OH)_2)$, thus more SnO_2 granules are also expected to be produced in the colloidal medium. The higher concentration of small SnO_2 granules, with increasing pH value of the solution, may be responsible for the generation of larger sized SnO_2 nanoparticles. Meanwhile, the low temperature synthesis controls the morphology of so-formed SnO_2 nanoparticles. Our XRD and TEM results are in very good agreement with this synthesis mechanism. On the other hand, the grain-growth mechanism in annealed nanoparticles may follow the diffusion process, where particles undergo multiple collisions leading to agglomeration and growth. The rate, at which agglomeration occurs primarily, depends on number of particles (initial concentration) and their mobility [27]. Agglomeration rate (R_f) is given by $R_f = k_f n_0^2$, where n_0 is initial concentration of small nanoparticles and $k_f = 4k_BT/3\eta$, where k_B is Boltzman constant, T is temperature and η is the viscosity of the medium. As the particle size decreases towards the molecular level, their behavior is more like vapor. The kinetic behavior of nanoparticles may follow the basic law of gaseous diffusion. Due to increase in the temperature, the rate of agglomeration process increases substantially leading to aggregated distribution of nanoparticles. This aggregated distribution of nanoparticles is clearly visible in TEM image of annealed sample (see fig. 2 c). This aggregated/larger size is responsible for the small band gap, comparatively sharper XRD peaks and diamagnetic contribution in the SnO_2 nanoparticles. Here we believe that the ferromagnetic contribution at low field values may be arising due to the presence of oxygen vacancies in the system and the diamagnetic behavior is attributed to their larger size. The observed ferromagnetic signals from un-doped oxide nanoparticles are still a matter of debate and sufficient research has to be focused in this area.

4. Conclusions

Single phase and spherical shaped tin oxide nanoparticles have been synthesized using wet chemical method. The size of nanoparticles was engineered via changing the pH value of the solution and post annealing treatment in air. The FWHM was found to decrease with increasing particle size. The experimental results infer that all the structural, optical and magnetic properties strongly depend on particle size. Room temperature ferromagnetism has been observed in 3pH grown SnO_2 nanoparticles. Optical band gap and ferromagnetic contributions were observed to decrease with increasing particle size.

Acknowledgements

Authors are thankful to material science group, Inter University Accelerator Center (IUAC), New Delhi for providing experimental facilities. One of the authors (Aditya Sharma) is grateful to IUAC, New Delhi, for

providing financial support under the UFUP project (code no. 41304).

References

[1] C. T. Campbell, S. C. Parker, D. E. Starr, Science **298**, 811 (2002).
[2] K. L. Merkle, L. J. Thompson, Phys. Rev. Lett., **88**, 225501(2002).
[3] V. T. Sven, N. L. Christost, L. Hartmut, Phys. Rev. Lett. **100**, 108302 (2008).
[4] D. Moldovan, V. Yamakov, D. Wolf, S. R. Phillport, Phys. Rev. Lett. **89**, 206101(2002).
[5] E. J. H. Lee, C. Ribeiro, T. R. Giraldi, E. Longo, E. R. Leite, J. A. Varela, Appl. Phys. Lett. **4**, 1745 (2004).
[6] Z. Wang, H. L. Li, Appl. Phys. A **74**, 201 (2002).
[7] X. H.Kong, X. M.Sun, X. Li, Mater. Chem. Phys. **82**, 997 (2003).
[8] H. W. Liang, Y. M. Lu, D. Z. Shun, B. H. Li, Z. Z. Zhang, C. X. Shan, J. Y. Zhang, X. W. Fan, G. T. Du, Solid State Commun. **137**, 182 (2006)
[9] D. Menzel, A. Awada, H. Dierke, J. Schoenes, F. Ludwig, M. Schilling, J. Appl. Phys. **103**, 07D106 (2008).
[10] G. Feng, W. Shufen, C. Hongming, L. Chunzhang, Nanotechnology **19** (2008) 095708.
[11] S. Kumar, Y. J. Kim, B. H. Koo, S. Gautam, K. H. Chae, R. Kumar, C. G. Lee, Mater. Lett. **63,** 194 (2009).
[12] I. S. Elfimov, S. Yunoki, G. A. Sawatzky, Phys. Rev. Lett. **89**, 216403 (2002).
[13] S. Zhou, E. Cizmar, K. Potzger, M. Krause, G. Talut, M. Helm, J. Fassbender, S. A. Zvyagni, J. Wasnitza, H. Schmidt, Phys. Rev. B **79,** 113201 (2009).
[14] Y. Zuo, S. Ge, Y. X. Zhau, X. Zhuo, Y. Xiao, L. Zhang, J.Appl. Phys. **104**, 023905 (2008).
[15] A. Sundersan, R. Bhargavi, N. Rangarajan, U. Siddesh, C. N. R. Rao, Phys. Rev. B **74**, 161306(R) (2006).
[16] M. Batzill, U. Diebold, Prog. Sur. Sci. **79**, 47 (2005).
[17] S. Tsunkawa, K. Ishikawa, Z. Q. Li, Y. Kawazone, A. Kasuya, Phys. Rev. Lett. **85**, 3440 (2000).
[18] S. Das, S. Kar, S. Choudhary, J. Appl. Phys. **99**, 114303 (2006).
[19] M. Venkatesan, C. B. Fitzgerald, J. M. D. Coey, Nature (London) **430**, 630 (2004).
[20] N. H. Hong, J. Sakai, N. Poirot, U. Brize, Phys. Rev. B **73**, 132404 (2006).
[21] D. Yoon, Y. Chen, A. Yang, T. L. Goodrich, X. Zuo, D. A. Arena, K Ziemer, C. Vittoria, V. G. Harris, J. Phys: Condens. Matter, **18** L, 355 (2006).
[22] N. H. Hong, N. Poirot, J. Sakai, Phys. Rev. B **77**, 033205 (2008).
[23] N. H. Hong, J. Sakai, U. Brize, J.Phys: Condens. Matter. **19**, 036219 (2007).
[24] J. Hays, A. Punnoose, R. Baldher. M. H. Engelhard, J. Peloquin, K. M. Reddy, Phys. Rev. B **72**, 075203 (2005).
[25] A. Sundersan, C. N. R. Rao, Nanotuday **4**, 96 (2009).
[26] F. H. Jones, R. Dixon, J. S. Foord, R. G. Egdell, J. B. Phetica, Surf. Sci. **376** 367 (1997).
[27] T. Mohanti, Y. Batra, A. Tripathi, D. Kanjilal. J. Nanosci. Nanotechnol. **7**, 2036 (2007).
[28] L. Jiang, G. Sun, Z. Zhou, S. Sun, Q. Wang, S. Yan, H. Li, J. Tian, J. Guo, B. Zhou, Q. Xin, J. Phys. Chem B **109**, 8774 (2005).

*Corresponding author: adityaiuac@gmail.com